Iranian Journal of Materials Science and Engineering, Vol. 19, Number 1, March 2022
RESEARCH PAPER

Tribology and Electrochemical Behavior of CrN/ZrN Multilayer Coatings Produced by Arc-PVD

Parviz Mohamadian Samim[1], Arash Fattah-alhosseini[2,*], Hassan Elmkhah[2], Omid Imantalab[2]

**a.fattah@basu.ac.ir*

[1] Department of Materials Engineering, Technical and Vocational University (TVU), Tehran, Iran
[2] Department of Materials Engineering, Bu-Ali Sina University, Hamedan 65178-38695, Iran

Received: September 2021 Revised: December 2021 Accepted: January 2022

DOI: 10.22068/ijmse.2482

Abstract: *In this study, CrN/ZrN multilayer nanostructured coatings with different bilayers (10, 20, and 30) were fabricated by the cathodic arc evaporation. The electrochemical behavior of samples was evaluated by polarization and impedance spectroscopy tests in the Ringer medium. In addition, the pin on disk test was used to investigate the tribological behavior of the samples. The results showed that the electrochemical and tribological behavior of the coatings were dependent upon the number of bilayers such that with the increase in the number of bilayers, the coatings showed higher corrosion resistance and better tribological performance. Field emission scanning electron microscopy (FE-SEM) images of the specimens after exposure to the corrosion medium showed that the number of surface cavities formed on the coatings with the highest number of bilayers were few in number and smaller in diameter. The results of the pin on disk test showed that by increasing the number of bilayers from 10 to 30, the coefficient of friction and wear rate decreased and the 30L coating showed better wear resistance.*

Keywords: *multilayer nanostructure, bilayers, CrN/ZrN, cathodic arc evaporation-physical vapor deposition (Arc-PVD), tribological behavior.*

1. INTRODUCTION

Creating surface coatings by different depositions methods is very important to improve the mechanical, tribological, and electrochemical behavior of metals and alloys [1]. Nitride coatings of transition metals, mostly based on Ti, Cr, and Zr, have been used to resist against corrosion and wear. Low friction coefficient, high melting point and hardness, high chemical stability, and good corrosion performance are the characteristics of these coatings [2]. Multilayer nitride coatings such as TiN/CrN, TiN/ZrN, TiN/NbN, and CrN/NbN have been of interest to researchers in recent years [3–6] that have properties such as high hardness, good mechanical strength, excellent adhesion, oxidation resistance, and corrosion, heat resistance and abrasion behavior [3, 4, 6–8]. The superiority of multilayer coatings in comparison to monolayer coatings is related to the fine structure and the large number of seasons in multilayer coatings [9]. Nano-scale multilayer structures are typically designed and created by repeating alternating layers with different architectures from different materials on the surface of tools and components. In these structures, the thickness of each bilayer plays a crucial role in their properties, and adjusting the thickness of each bilayer is an important factor in improving properties such as wear. In addition, the design of the structure, for example, grain size, morphology, as well as the number of interfaces, optimizes the physical properties of nanolayer coatings [9].

The cathodic arc evaporation-physical vapor deposition (Arc-PVD) is a desirable method to deposit nitride multilayer coatings that has been used in various applications [10, 11]. Good adhesion to the substrate, high hardness, homogeneity, high density and better properties comparing with created coatings by magnetron sputtering are the characteristics of coatings created by the Arc-PVD method [12]. By this method, it is possible to create all kinds of coatings like metal carbide, metal nitride, and pure metals. Different gases are added to the coating chamber depending on the type of the deposited coating. Argon gas is used to apply metal coatings and nitrogen is used to apply nitride coatings on metals. It should be noted that the coatings produced by the Arc-PVD method have a columnar structure and the presence of micropores between the columns is an inherent disadvantage of this method. In addition, the

[DOI: 10.22068/ijmse.2482]

presence of macroparticles (metal droplets returning from cathodic points) in the total volume of the coating and grain boundaries are other known defects of this method [12]. The presence of these defects in the coating influences the mechanical and corrosion properties of the coated components. According to what was mentioned, an effective method to improve the quality of the coating is to create multilayer coatings because the growth of the column with this method is limited or even stopped, and as a result, the possibility of crevice corrosion along the columns is decreased.

CrN coating exhibits excellent oxidation and corrosion resistance in addition to wear properties. On the other hand, high hardness, wear resistance, corrosion resistance and good thermal stability are the characteristics of ZrN coating. Thus, it can be said that the multilayer coatings composed of the mentioned nitrides produce a combination of desirable chemical and mechanical properties [7]. The main reasons for using CrN/ZrN multilayer coatings are high hardness and good wear properties of both nitrides and limiting column growth with alternative deposition of CrN/ZrN [8].

Based on the published papers, limited studies have been carried out on the corrosion behavior of CrN/ZrN multilayer nanostructured coatings comparing with other nitride multilayer coatings and most studies have been on their wear, mechanical, and thermal stress properties [13, 14]. The purpose of this study is to create a CrN/ZrN multilayer nanostructured coating (with different bilayers) using the Arc-PVD method and to study the relationship between their electrochemical and tribological behavior with the number of interfaces created in the coating or in other words the coating architecture. The electrochemical behavior of the created coatings in the Ringer medium was studied.

2. EXPERIMENTAL PROCEDURE

In this study, CrN/ZrN multilayer nanostructured coatings with bilayers of 10 (10L), 20 (20L), and 30 (30L) were created by the Arc-PVD method. The deposition process parameters are indicated in other papers published by this research team [15]. The multilayer nanostructured coatings were created on 304 stainless steel substrate with dimensions of 40 × 40 × 1 mm. In order to prepare the surface before applying the coating, the surface of the substrates was sanded using abrasive papers with abrasive particles of SiC material (from 100 to 5000). Thus, the polishing operation was performed and at last, using an ultrasonic device, degreasing of the specimen surface in ethanol bath was performed.

Diffraction was performed using the Philips PW1730 X-ray diffraction (XRD) and the XRD pattern was analyzed using X'Pert HighScore Plus software. Electrochemical studies were carried out in Ringer's solution (with a composition of 8.60 g/cm^3 sodium chloride, 0.3 g/cm^3 potassium chloride, and 0.48 g/cm^3 calcium chloride) at ambient temperature. Electrochemical tests including potentiodynamic polarization (PDP) and electrochemical impedance spectroscopy (EIS) experiments were performed using μAUTOLABIII/FRA2 equipped with Nova 1.11 software. The PDP test started at -250 mV according to the corrosion potential at a scan rate of 1 mV/s and continued until the passive surface area. EIS tests were carried out in the 100 kHz to 10 mHz frequency range with an alternating and sinusoidal signal amplitude of ten millivolts in open-circuit potential. The Mira 3 TESCAN Model FE-SEM was used in order to evaluate the microstructure of the coating and to evaluate the corroded surfaces of the samples. In order to evaluate the tribological behavior of the samples, the rotating pin-on-disk method was used in an alumina ball with a diameter of 10 mm as an abrasive item. This test was performed under the applied force of 3 N, slipping speed of 0.2 m/s, and slip distance of 500 m (in dry conditions or without lubricant) at room temperature. Microscopic examinations of the effect of wear were performed using a scanning electron microscope of the JEOL 20 KV model. In order to evaluate the mechanical behavior, a TriboScope® Nanomechanical Test Instrument with 2D transducer was used, equipped with a Berkovich indentor (from five different points with a force of 6000 μN and a distance of 200 μm). Then, NanoScope version 3.5.4.4 software was used to extract the information.

3. RESULTS AND DISCUSSION

3.1. Microstructure of coatings

Fig. 1 indicates the FE-SEM images using the backscattered electrons from the cross-section of

[DOI: 10.22068/ijmse.2482]

the multilayer nanostructured coatings. According to this figure, it is obvious that under all multilayer coatings, there is a layer of chromium that is owing to the existence of this interlayer to create the desired adhesion of the coating to the substrate [6].

Also, microstructural multilayers at the nanoscale are easily visible. In the images shown in Fig. 1, the ZrN layers and the CrN layers of the multilayer coatings are bright and dark, respectively, due to the difference in the atomic numbers of chromium and zirconium and its effect on the backscattered electrons intensity [16]. Furthermore, the difference in the evaporation rate of the target material in the same current has made the thickness of ZrN layers in the multilayer nanostructured coatings to be thicker than the CrN layers [7]. The existence of smooth and free of any effect of waving layers in the images shown in Fig. 1 indicates that the structure of the coating layers is dense and compact.

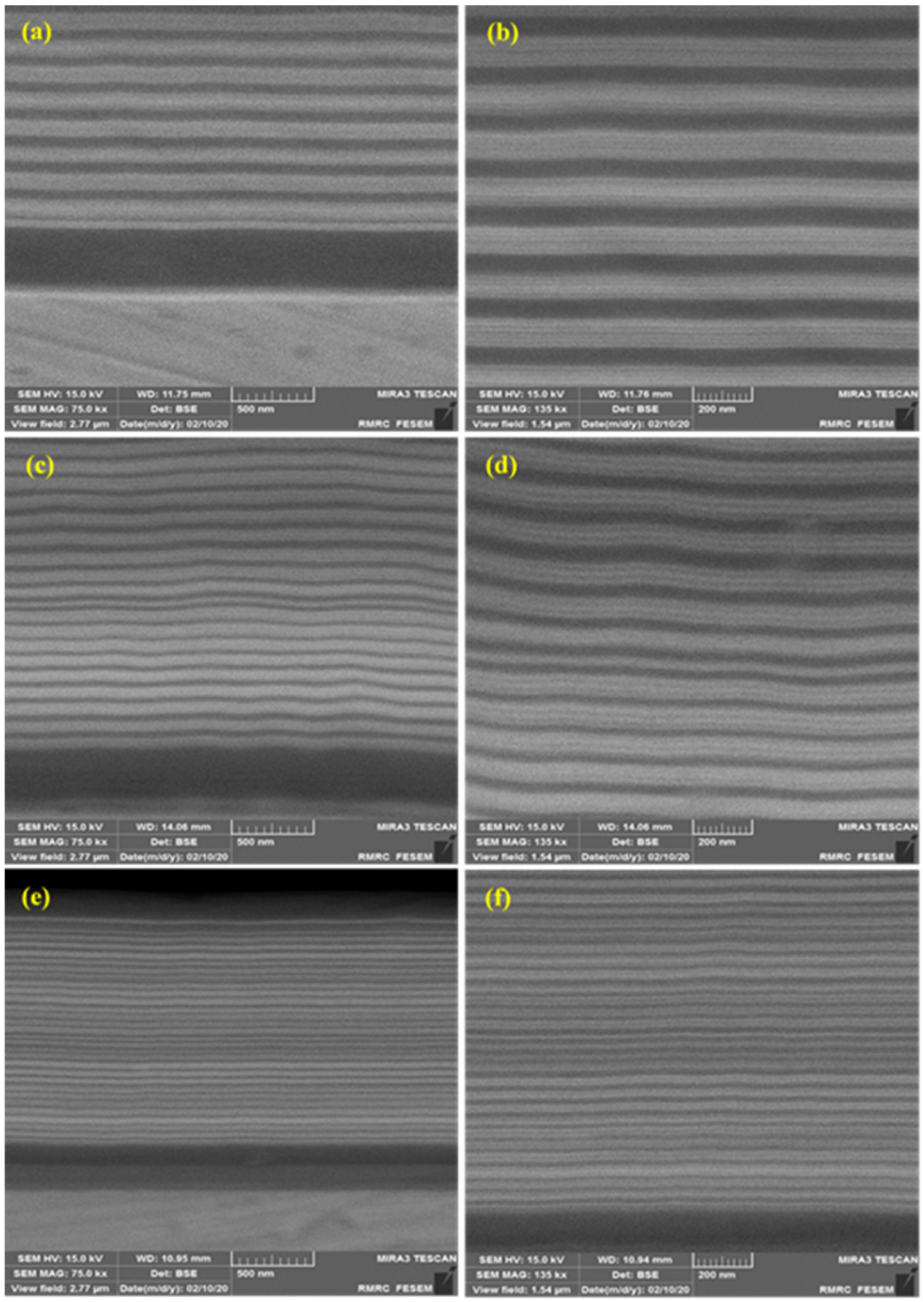

Fig. 1. FE-SEM images of cross-section of CrN/ZrN nanostructured coatings: (a, b) 10L, (c, d) 20L and (e, f) 30L.

[DOI: 10.22068/ijmse.2482]

Also, according to the topography of the images presented in Fig. 1, it can be seen that no sign of macroparticles that are considered as inherent defects of coatings created by the Arc-PVD method, is seen in the section of coatings. Nevertheless, inherent defects in the Arc-PVD coating, including macroparticles and pinholes were seen in the surface images of the coatings (reported in the next sections). It should be noticed that the existence of macroparticles and pinholes can affect the electrochemical and tribological behavior of the applied coatings.

3.2. XRD pattern

Fig. 2 depicts the results of the XRD test for CrN/ZrN multilayer nanostructured coatings. According to the obtained patterns, it is obvious that the texture of the coating depends on the type of coating and the results show that the CrN/ZrN multilayer nanostructured coatings (based on the standard cards (JCPDFs) with the numbers 96-900-8468, 96-901 -6423, 96-430-3946 and 96-900-8779) has FCC crystal structure of B1-NaCl type.

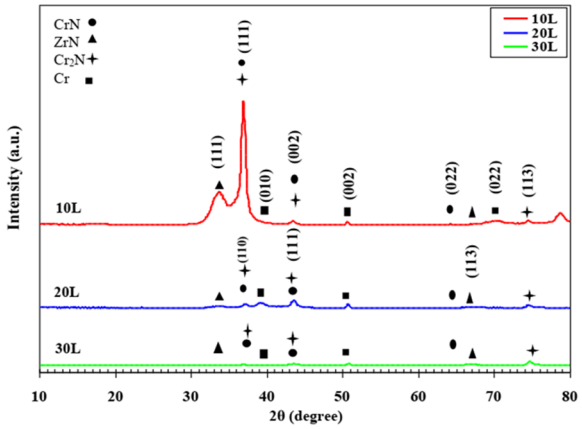

Fig. 2. XRD patterns of 10L, 20L, and 30L nanostructured coatings deposited on AISI 304.

In addition, the analysis of the obtained diffraction patterns using X'Pert HighScore Plus software showed the orientation of plans (111), (002), and (222) related to CrN, plans (111), (002), and (113) related to ZrN, (002) related to Cr and (113) related to Cr_2N. Similar results have been reported by other researchers [9, 14, 17]. By Scherer formula (Eq. 1), the size of ZrN and CrN crystallite related to multilayer nanostructured coatings was calculated using the full width at half maximum (FWHM) [7, 14, 17], that the obtained results are summarized in Table 1.

$$D = 0.9\lambda/\beta \cos\theta \quad (1)$$

In the Scherer equation (Eq. 1), D is the mean size of the crystal, λ denotes the wavelength of the X-ray, and θ is the diffraction angle.

Table 1. Crystallite size of CrN and ZrN in ZrN/CrN nanostructured coatings deposited on AISI 304

Sample		10L	20L	30L
Crystallite size (nm)	CrN	12.4	10.6	6.6
	ZrN	6.4	5.6	6

3.3. Electrochemical behavior

The usual test to evaluate and compare the corrosion resistance of multilayer coatings is the EIS measurement that is a fast, impressive, surface-sensitive, and non-destructive method [18]. Fig. 3 presents the experimental results of the EIS tests for multilayer nanostructured coatings, after 168 h of immersion under open-circuit potential conditions in Ringer's solution, in the form of Nyquist and Bode diagrams.

According to the Nyquist curve presented in Fig. 3, the capacitive behavior of all of these three coatings is clear. In addition, the diameter of capacitive arcs has increased from 10 to 30 as the number of bilayers rises. The corrosion resistance of the created coatings depends on the diameter of the capacitive arcs and the larger the diameter of the capacitive arcs in the Nyquist diagram, the greater is the corrosion resistance [18]. Based on the Bode-module diagram illustrated in Fig. 3, the total impedance value of the 30L specimen is higher than that of the 10L and 20L specimens that is in perfect agreement with the presented Nyquist diagram. Also, the non-dependence of the total impedance value on the frequency in the high-frequency ranges (more than 10 kHz) shows the pure resistance behavior. The pure resistance behavior can be observed in the Bode-phase diagram with no dependence of the phase angle on the frequency. According to the Bode-phase diagrams in Fig. 3, the 30L sample indicates a wider region in comparison to other specimens at high phase angles that indicates a higher resistance value of the sample and better capacitive behavior [19]. Also, the existence of two-time constants or two constant phase elements (CPE) in the range of less than 10 kHz (medium and low-frequency range) is detectable for all three multilayer nanostructured coatings.

[DOI: 10.22068/ijmse.2482]

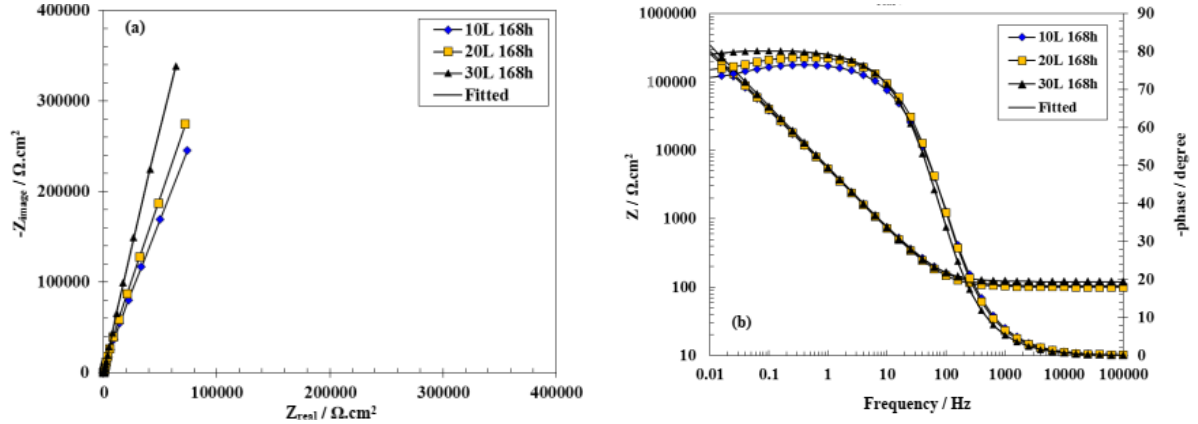

Fig. 3. (a) Nyquist and (b) Bode plot of 10L, 20L, and 30L on AISI 304 substrate.

Phase angle amplitude at angles of about -80° as well as slope -1 in the wide frequency range is ascribed to capacitive behavior and great corrosion resistance. These parameters can reflect the homogeneity of the surface, high density of the coating and its low defects [20]. It should be noticed that the deviation from the ideal state of the capacitor using the Bode-phase curve is quite obvious. Thus, the existence of CPE in the proposed electrical equivalent circuit (EEC) is necessary to simulate the experimental EIS data. In the present study, the EEC presented in Fig. 4 was utilized in order to simulate the experimental data of EIS. Other researchers have used this EEC in order to simulate EIS experimental data related to single-layer and multilayer coatings created by the Arc-PVD method [15, 21, 22].

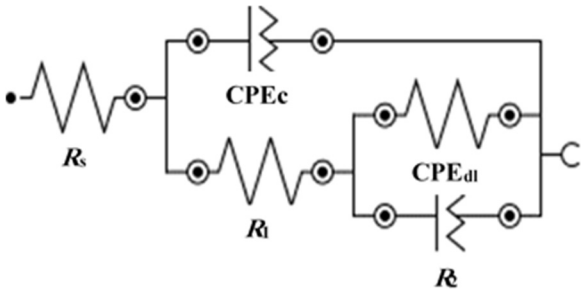

Fig. 4. EEC for the simulation of the EIS plots of CrN/ZrN nanostructured coatings.

In the circuit presented in Fig. 4, R_s, R_1, and R_2 are ascribed to solution resistance, coating resistance, and electron transfer resistance, respectively. CPE_C is the CPE for coatings and CPE_{dl} is the CPE for the electrical double layer. The CPE impedance (Z_{CPE}) is defined as below (Eq. 2):

$$Z_{CPE} = 1/Q(j\omega)^n \quad (2)$$

Where Q is the CPE with unit $S^{\alpha}/\Omega.cm^2$, j is the imaginary part, ω shows the angular frequency with rad/sec and n is the surface uniformity coefficient. The parameters n and Q are frequency-independent [23]. Table 2 summarizes the values of the electrical parameters obtaining from the simulation of the EIS experimental data (presented in Fig. 3).

Table 2. Values of EEC elements corresponding to CrN/ZrN nanostructured coatings deposited on AISI 304 as a function of immersion time in Ringer media

Sample	10L	20L	30L
Immersion time (h)	168	168	168
R_s ($\Omega.cm^2$)	104.32	100.81	101.22
Q_c ($\times10^{-4}$ $S^{\alpha}/\Omega cm^{-2}$)	0.40	0.31	0.34
n_1	0.86	0.88	0.89
R_1 ($M\Omega.cm^2$)	1.60	1.00	1.56
Q_{dl} ($\times10^{-4}$ $S^{\alpha}/\Omega.cm^{-2}$)	0.13	0.43	0.06
n_2	0.78	0.74	0.62
R_2 ($M\Omega.cm^2$)	10.72	19.50	20.31
$R_p=R_1+R_2$ ($M\Omega.cm^2$)	12.32	20.50	21.78

According to Table 2, the highest polarization resistance (total of R_1 and R_2) among the studied nanostructured coatings is related to the 30L sample and it is clear that the polarization resistance has increased by rising the number of bilayers. The better behavior of 30L nanostructured coatings can be ascribed to the effect of the interface on the corrosion behavior of multilayer coatings. In other words, rising the interfaces in the multilayer nanostructured coating reduces penetrable defects such as pores, cracks, and pinholes in the coating by alternating deposition of CrN and ZrN layers and blocks the penetration of corrosive agents by making a denser structure and raises corrosion resistance of the coating [20, 24]. Researchers believe that the

[DOI: 10.22068/ijmse.2482]

resistance of the coating is inversely related to the content of defects in the coating and higher values of the resistance of the coating show a higher density of the coating [20]. In order to validate the EIS experimental data, Kramers-Kronig transformations are used that convert real axes to imaginary axes and imaginary axes into real axes [25]. Comparing the Kramers-Kronig transformations with the EIS experimental data of the created coatings (Fig. 5) in the Ringer solution shows that the experimental data are in good agreement with the Kramers-Kronig transformations and that the coatings were stable under the EIS test and met the theoretical requirements of the linear system [26]. Other publications of the scientific papers [27–29] provide more details on the Kramers-Kronig curves. Fig. 6 shows the PDP curves of the studied specimens after 168 h of immersion in a Ringer solution under the conditions of open-circuit potential. The corrosion current density (i_{corr}) and corrosion potential (E_{corr}) for all three coatings were extracted by Fig. 6 and are summarized in Table 3. The corrosion current densities obtained from plots of PDP using the method of Tafel linear extrapolation [18]. Comparing the data reported in Table 3, the values of corrosion current density tended to lower values and the values of corrosion potential tended to more noble values by increasing the number of interfaces related to the created coatings, showing a rise in corrosion resistance of the coating by increasing number of interfaces [30]. Thus, it can be said that due to rise in the number of interfaces due to re-nucleation led to blocking the amount of inherent defects in the coating created by the Arc-PVD process. Studies by other researchers suggest that increase of bilayers in multilayer coatings reduces the percentage of cavities in the coating and thus increases its density [31]. As mentioned earlier, interfaces in multilayer coatings can act as a barrier against electrolyte penetration and limit its path to the substrate in addition to reducing the possibility of cavity formation. Similar results have been reported by other researchers for multilayer coatings applied by PVD methods [32]. In general, the increase in corrosion performance in multilayer coatings can be attributed to the dense structure, without cracks, non-columnar microstructure, and fine-grained [20].

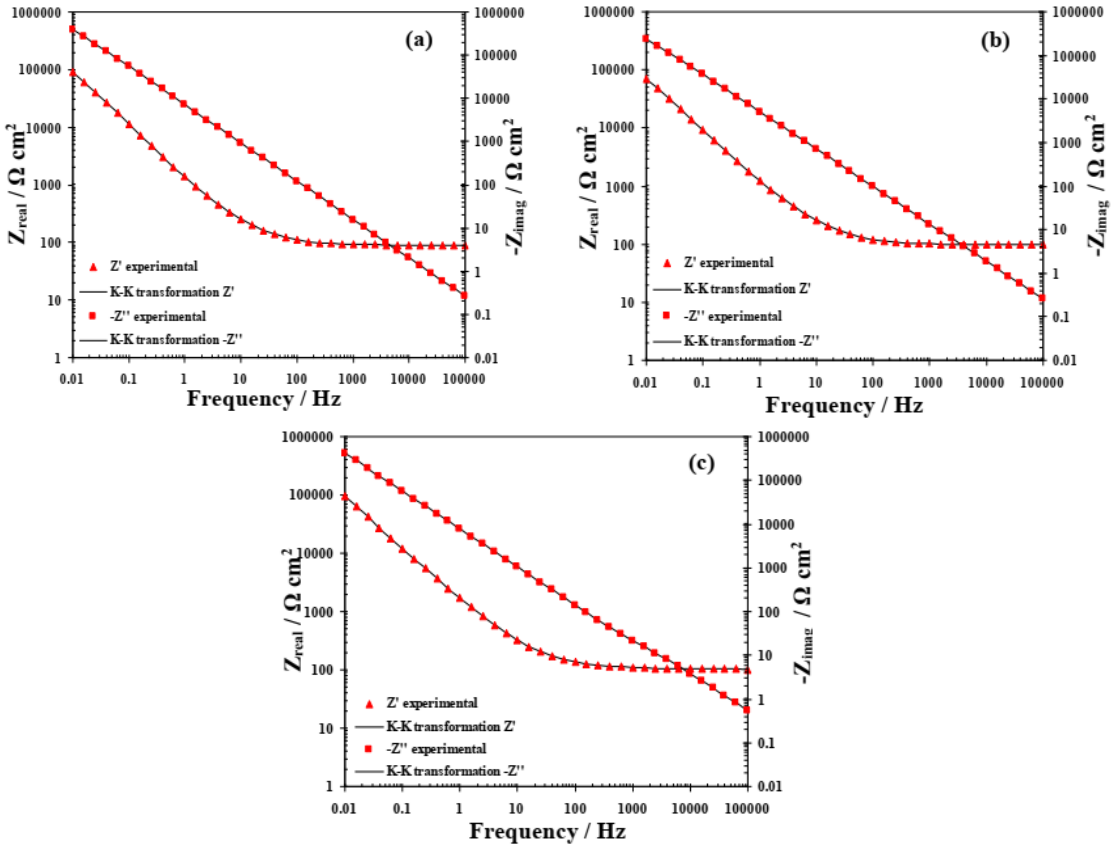

Fig. 5. Kramers-Kronig transformations of (a) 10L, (b) 20L, and (c) 30L after 168 h immersion in Ringer media.

[DOI: 10.22068/ijmse.2482]

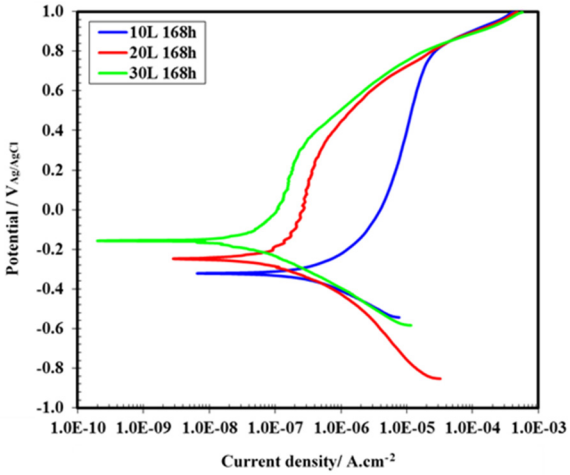

Fig. 6. PDP plots of 10L, 20L and 30L after 168 h immersion in Ringer media.

Table 3. E_{corr} and i_{corr} corresponding to CrN/ZrN nanostructured coatings deposited on AISI 304 samples in Ringer media

Sample	10L	20L	30L
Immersion time (h)	168	168	168
E_{corr} ($V_{Ag/AgCl}$)	-0.321	-0.246	-0.157
i_{corr} ($A.cm^{-2}$)	2.32×10^{-7}	5.08×10^{-8}	1.76×10^{-8}

3.4. Observation of the sample's surface after electrochemical measurements

In order to assess the surface morphology of the samples (before and after electrochemical tests), the images shown in Fig. 7 were used.

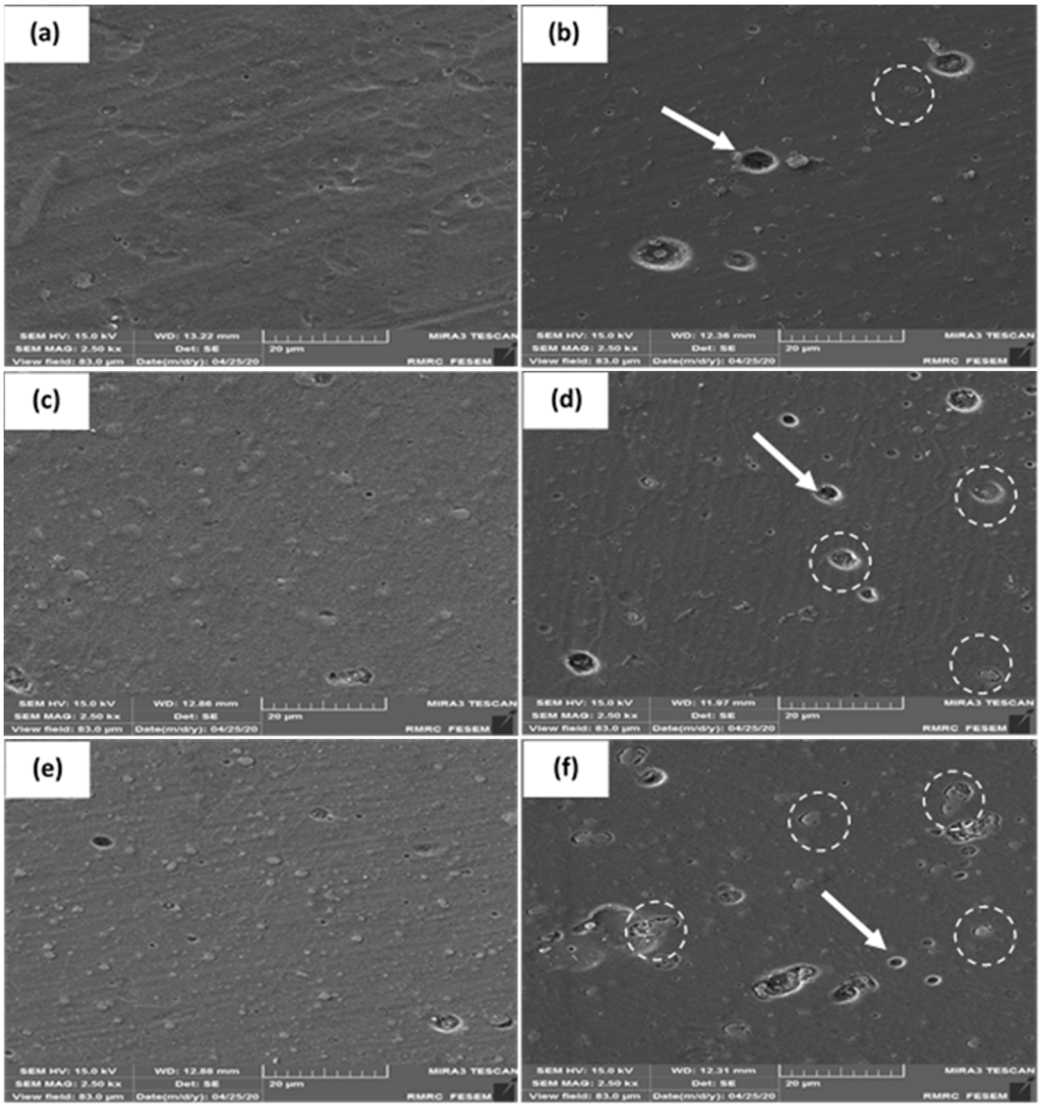

Fig. 7. FE-SEM images of planer of CrN/ZrN nanostructured coatings before and after immersion in Ringer media: (a, b) 10L, (c, d) 20L, and (e, f) 30L.

[DOI: 10.22068/ijmse.2482]

According to the surface images of the samples before immersion, the existence of macroparticles and pinholes can be seen as inherent defects within the Arc-PVD coating procedure. Within the coating procedure, the arc discharges onto the target surface have formed metal macroparticles that are then sprayed onto the surface of the coating. Dispersion of particles leads to the formation of areas called pinholes [10]. According to the surface images after electrochemical tests, it can be seen that the 30L coating has corrosion cavities with a smaller number and smaller diameter (arrow mark) in comparison to what the 10L and 20L coatings have shown. Moreover, 20L coatings show smaller corrosion holes comparing with 10L coatings. Nevertheless, some areas are marked with a dashed circle in the images of all three coatings that are related to the macroparticles resulting from the deposition process. These results are consistent with obtained data from EIS tests and PDP.

3.5. Nanoindentation

Fig. 8 shows the displacement-force curves from the nanoindentation test for 10L, 20L, and 30L multilayer nanostructured coatings. The area of sub-curves in loading and unloading is defined as plastic deformation work (W_p) which can be used to evaluate the plastic deformation resistance and wear resistance of multilayer nitride coatings [33]. In general, increasing the strength of the material results in a decrease in toughness. However, the reported results in published scientific papers on TiN/CrN multilayer coatings show that the increase in hardness in multilayer coatings was not related to a decline in toughness [33]. Multilayers that have a lower displacement load curve area show less plastic deformation work and more plastic deformation resistance [33]. Based on the indicated diagrams in Fig. 8, it can be seen with the rise in the number of bilayers that shifts to left there is an increase in resistance to deformation [34].

The amount of hardness and the effective Young's modulus for the created coatings are summarized in Table 4. According to the reported values, it is clear that with increasing the number of interfaces in the coating or in other words increasing the rotation speed in the sample during the coating process, the hardness (H) and the effective Young modulus (E^*) of the created coating increased. The results are in good agreement with the reported results by other researchers on CrN/ZrN multilayer coatings [2, 16]. The increase in hardness and effective Yang modulus is understandable according to the coating structure. Nanolayer coatings and the creation of an interface in the coating are solutions to increase the hardness of the coating because the interfaces of the CrN/ZrN multilayer coating can be barriers to dislocation slip and grain column growth between the layers. Clearly, locking dislocations due to coherent strains for different nanocrystalline grains contributes to the increase in hardness. In the other words, the preferred orientations for the strong mixture of Zr-N and Cr-N are in the way that they create higher hardness and modulus [2].

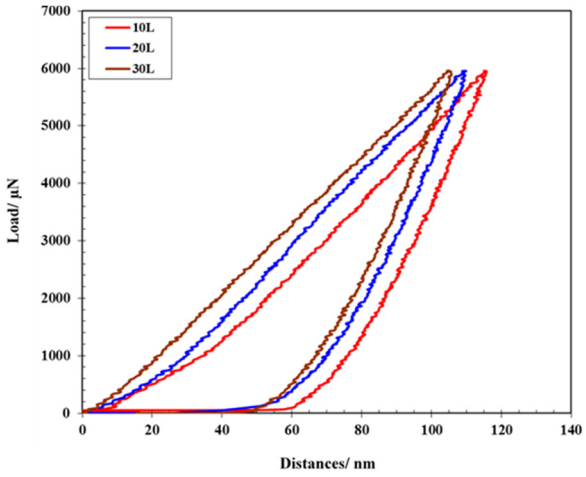

Fig. 8. Nanoindentation plots of 10L, 20L, and 30L coatings.

In order to assess the mechanical properties and predict the protective properties of the coating, hardness to Young modulus ratios can be used. For this purpose, the two parameters H/E^* and H^3/E^{*2} are the key parameters. H/E* ratio is a parameter that is used to determine the elastic behavior of the surface in contact with external forces. The protective behavior of the coating is characterized from the view of crack resistance, abrasion wear, and rating of coating toughness using this parameter [35]. According to the data in Table 4, the H/E^* index for 30L coating is higher than 10L and 20L coating. Thus, it can be said that this coating indicates better behavior in comparison to the 10L and 20L coatings against external forces, cracking, and resistance against elastic strain.

[DOI: 10.22068/ijmse.2482]

Table 4. Mechanical properties of CrN/ ZrN nanostructured coatings deposited on AISI 304.

Sample	10L	20L	30L
E^*	299±3.3	300±2.2	308±0.4
H	25±0.8	26±0.6	27±0.4
H/E^*	0.084	0.087	0.088
H^3/E^{*2}	0.175	0.197	0.209

The H^3/E^{*2} parameter, makes it possible to estimate and classify the coating in relation to plastic deformation. This ratio is calculated for the produced coatings in the present study and is reported in Table 4. The improvement of the reported mechanical parameters, hardness, and subsequent H/E^* and H^3/E^{*2} ratios, for the 30L sample compared with the 10L and 20L samples can be attributed to the reduction of the thickness of the bilayers followed by the reduction of the grain size which leads to increase the volume of the interfaces and increase the role of the boundaries as pinning points in the coating. Reducing the thickness of the layers, or in other words, increasing the interfaces leads to prevent the movement of dislocations (strengthening according to the well-known Hall-Patch relationship) and improves the strength and increases the hardness. The effective role of increasing the number of interfaces can be considered as a factor preventing the spread of cracks and dislocations and joining cavities and Pinholes [35]. According to the data in Table 4, 30L coating is supposed to show better properties in tribological uses and against wear [22].

3.6. Tribological behavior

Fig. 9 indicates a diagram of the changes in the friction coefficient in terms of sliding distance and the average value of the friction coefficient related to the substrates and created coatings in conditions of lubricant-free. According to Fig. 9 (a), it is quite clear that the friction coefficient of the substrate is higher in comparison to the created coatings. Typically, the friction coefficient is related to factors such as the actual contact area, debris, wear particles, the reaction layer, and the formation of the transition layer [36]. In addition, fluctuations in the friction coefficient of the curve are seen in terms of distance for all coatings that is attributed to the local failure of the layer and the formation of tribolayer [36].

The unstable step of the friction coefficient may be affected by high humidity or other environmental factors during the test [37].

According to the mean values of the friction coefficient that were reported in Fig. 9 (b), the least value is related to the 30L coating and shows a decreasing trend by rising the number of interfaces in the coating [36]. The lowest coefficient friction of the 30L specimen can be attributed to its higher hardness compared to other specimens. It is known that hardness has an important effect on the wear behavior of materials [38]. Higher hardness leads to higher load-bearing capacity and lower actual contact surface with the opposite surface.

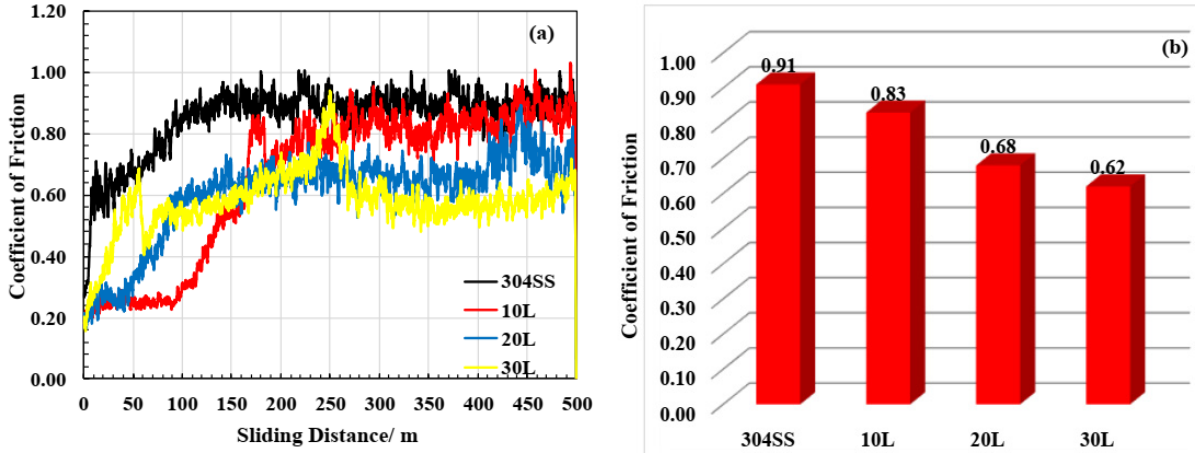

Fig. 9. (a) Friction coefficient-sliding distance plots and (b) friction coefficient of 10L, 20L, 30L, and AISI 304.

[DOI: 10.22068/ijmse.2482]

Under the same wear conditions, according to Archard's law, the wear rate is inversely related to hardness [38]. Research by other researchers has shown that the multilayer AlTiN/AlCrSiN coating produced with higher hardness and higher H/E^* ratio has a higher adhesion strength [39] that indicates higher resistance against cracking.
The results obtained, means the decreasing trend of the friction coefficient can be related to the improvement of mechanical properties due to the effect of interface and elastic recovery by increasing the number of bilayers [34, 40, 41]. The reduction of the friction coefficient in 30L coatings can be interpreted according to the mechanical friction model proposed by Archard. According to this model (Eq. 3), the friction coefficient is related to the numerical amount of roughness and elastic-plastic behavior of the coating [34]:

$$\mu = \frac{F_t}{F_n} = C_k \times \frac{R(s)}{\sigma_{t\,(H \cdot Er)}} \quad (3)$$

In this equation, μ is the friction coefficient in the system, C_k is a constant depending on the test conditions, R(s) shows the roughness of the coating, $\sigma_{(H.Er)}$ is a variable that includes the elastic and plastic properties of the coating. According to Archard's model, when the coating has higher hardness and lower roughness, the friction coefficient starts with a smaller value and stabilizes over long slip distances [34, 41]. The values of roughness for the coatings are shown in Table 5. Thus, due to these two effective factors, the decreasing trend of the friction coefficient can be inferred by increasing the number of bilayers from the sample of 10L to the specimen of 30L.

Table 5. Roughness of CrN/ZrN nanostructured coatings deposited on AISI 304

Sample	10L	20L	30L
Ra (nm)	33.7	19.5	9.1

Table 6 shows the numerical value of the wear rate for 10L, 20L, 30L coatings and 304 steel substrate after 500 meters of wear distance. As can be seen, multilayer coatings show different wear rates. So, by increasing the number of bilayers, the wear rate shows a decreasing trend. Thus, the 30L coating has the most amount of wear resistance. The low wear rate of the 30L coating is attributed to its higher hardness than other coatings and substrates. Since according to Archard's relationship, the volume of lost material decreases by increasing hardness in the coating [42]. According to the information in Fig. 9 and Table 6, it can be said that the wear resistance behavior of all three coatings is better than the substrate. Also, by increasing the layer from 10 to 30, the wear resistance behavior has been improved that can be attributed to the higher hardness of the coatings in the multilayer coatings and the higher ratio of H^3/E^{*2} and H/E^* (Table 4) [40].

Table 6. Wear rate of CrN/ZrN nanostructured coatings deposited on AISI 304 and AISI 304 samples in dry condition

Sample	10L	20L	30L	304
Wear rate (mm^3/ N.m)	1.08×10^{-4}	6.22×10^{-6}	3.50×10^{-6}	2.30×10^{-3}

Fig. 10 shows the SEM images of the wear track at different magnifications for multilayer and substrate coatings. As can be seen and during slipping, several types of wear mechanisms may occur, such as adhesion, abrasion, and surface fatigue. In Fig. 10, the arrow symbol 1 indicates the parallel lines of the scratch that shows the wear mechanism of the abrasion. The arrow sign 2 indicates the material rubbed on the surface that shows the mechanism of adhesive wear. Also, the sign of arrow 3 shows a series of microcracks and scales that occur owing to surface fatigue on the surface. However, due to the high hardness of nanolayer coatings, the predominant wear mechanism is abrasive wear [43].
Multilayer coating with 30Layers showed a more desirable behavior that the reduction of its wear path size confirms the effect of more layers in the multilayer coating on the wear resistance of these coatings. Thus, the best performance against abrasion was observed in 30L coating and next in 20L coating, which can be attributed to the low friction coefficient, higher hardness, and low roughness with their multilayer structure that have more interfaces [37, 40].

4. CONCLUSIONS

CrN/ZrN nanostructured coatings with 10, 20, and 30 bilayers on 304 stainless steel substrates were applied by the Arc-PVD method. The following results were obtained by various tests performed on the samples:

[DOI: 10.22068/ijmse.2482]

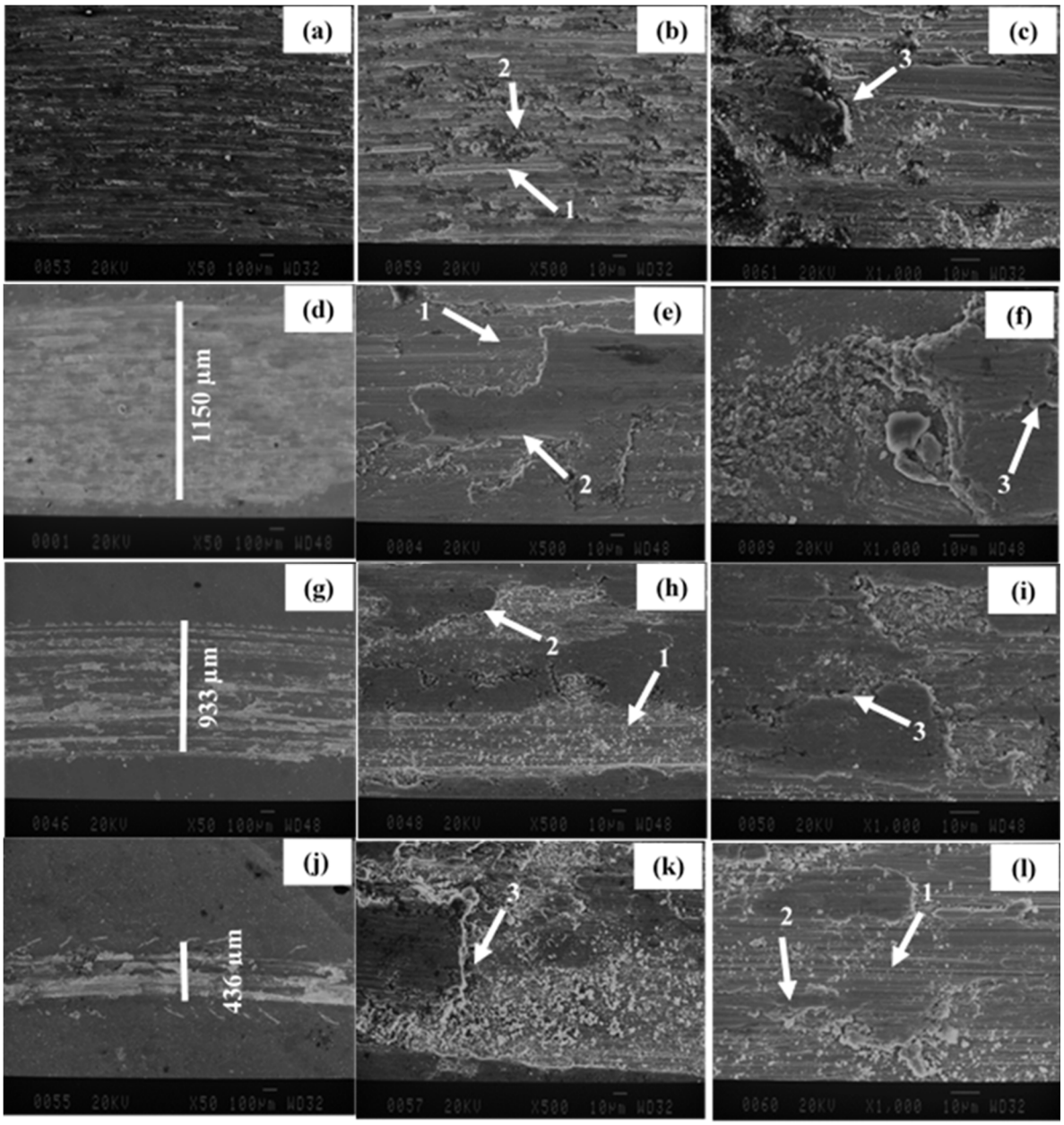

Fig. 10. SEM images on the wear tracks of ((a), (b) and (c)) AISI 304, ((d), (e) and (f)) 10L, ((g), (h) and (i)) 20L and ((j), (k) and (l)) 30L.

1. Studying CrN/ZrN multilayer coatings by FE-SEM images revealed that the prepared coatings had high density.
2. The results of PDP tests showed that by increasing the number of bilayers from 10 to 30Layers, the corrosion current density decreased from 2.332×10^{-7} to 1.761×10^{-8} A.cm^{-2} during 168 h in the Ringer solution.
3. The results of EIS tests showed that by changing the number of bilayers from 10 to 30 in CrN/ZrN multilayer nanostructured coatings, the polarization resistance in the Ringer medium increased from 12.32 to 21.87 MΩ.cm^2.
4. Decreasing the corrosion current density and increasing the polarization resistance in CrN/ZrN multilayer nanostructured coatings in the Ringer solution indicate the improvement of corrosion behavior that can be increased by increasing the interfaces and reducing the penetration paths of corrosive agents such as pores and cavities can be attributed to the increase in the number of bilayers.

[DOI: 10.22068/ijmse.2482]

5. The hardness of the 10L, 20L, and 30L coatings was 25, 26, and 27 GPa, respectively, and Young's modulus of the coatings was 298, 300, and 308 GPa, respectively.
6. Changes in the friction coefficient of CrN/ZrN multilayer nanostructured coatings showed a decreasing trend by increasing the number of bilayers and by increasing the number of bilayers from 10 to 30, the friction coefficient decreased from 0.82 to 0.62.
7. The wear rate in CrN/ZrN multilayer nanostructured coatings decreased by rising bilayers rate. By increasing the number of bilayers from 10 to 30, the wear rate decreased from 0.08×10^{-4} to 3.5×10^{-5} mm^3/Nm.

REFERENCES

[1] Beresnev, V. M., Bondar, O. V., Postolnyi, B. O., Lisovenko, M. O., Abadias, G., Chartier, P., Kolesnikov, D. A., Borisyuk, V. N., Mukushev, B. A., Zhollybekov, B. R., and Andreev, A. A., "Comparison of tribological characteristics of nanostructured TiN, MoN, and TiN/MoN Arc-PVD coatings." J. Frict. Wear, 2014, 35, 374–382.

[2] Zhang, J. J., Wang, M. X., Yang, J., Liu, Q. X., and Li, D. J., "Enhancing mechanical and tribological performance of multilayered CrN/ZrN coatings." Surf. Coatings Technol., 2007, 201, 5186–5189.

[3] Y. Purandare, M.M. Stack, P. H., "A study of the erosion–corrosion of PVD CrN/NbN superlattice coatings in aqueous slurries." wear, 2005, 259, 160–167.

[4] Maksakova, O. V., Simoẽs, S., Pogrebnjak, A. D., Bondar, O. V., Kravchenko, Y. O., Koltunowicz, T. N., and Shaimardanov, Z. K., "Multilayered ZrN/CrN coatings with enhanced thermal and mechanical properties." J. Alloys Compd., 2019, 776, 679–690.

[5] Abdeen, D., El Hachach, M., Koc, M., and Atieh, M., "A Review on the Corrosion Behaviour of Nanocoatings on Metallic Substrates." Materials (Basel)., 2019, 12, 210.

[6] Lin, C.-K. K., Hsu, C.-H. H., and Kung, S.-C. C., "Effect of electroless nickel interlayer on wear behavior of CrN/ZrN multilayer films on Cu-alloyed ductile iron." Appl. Surf. Sci., 2013, 284, 59–65.

[7] Maksakova, O., Simoẽs, S., Pogrebnjak, A., Bondar, O., Kravchenko, Y., Beresnev, V., and Erdybaeva, N., "The influence of deposition conditions and bilayer thickness on physical-mechanical properties of CA-PVD multilayer ZrN/CrN coatings." Mater. Charact., 2018, 140, 189–196.

[8] Vengesa, Y., Fattah-alhosseini, A., Elmkhah, H., Imantalab, O., "Influence of post-deposition annealing temperature on morphological, mechanical and electrochemical properties of CrN/CrAlN multilayer coating deposited by cathodic arc evaporation- physical vapor deposition process." Surf. Coatings Technol., 2022, 432, 128090.

[9] Zhang, Z. G., Rapaud, O., Allain, N., Mercs, D., Baraket, M., Dong, C., and Coddet, C., "Microstructures and tribological properties of CrN/ZrN nanoscale multilayer coatings." Appl. Surf. Sci., 2009, 255, 4020–4026.

[10] Huang, S. H., Chen, S. F., Kuo, Y. C., Wang, C. J., Lee, J. W., Chan, Y. C., Chen, H. W., Duh, J. G., and Hsieh, T. E., "Mechanical and tribological properties evaluation of cathodic arc deposited CrN/ZrN multilayer coatings." Surf. Coatings Technol., 2011, 206, 1744–1752.

[11] Maksakova, O. V., Pogrebnjak, A. D., and Simoes, S., "Morphology, Structure and Thermal Properties of Multilayer ZrN/CrN Coatings." IEEE 38th Int. Conf. Electron. Nanotechnol., 2018, 106–109.

[12] Gilewicz, A., Chmielewska, P., Murzynski, D., Dobruchowska, E., and Warcholinski, B., "Corrosion resistance of CrN and CrCN/CrN coatings deposited using cathodic arc evaporation in Ringer's and Hank's solutions." Surf. Coatings Technol., 2016, 299, 7–14.

[13] Chen, S. F., Kuo, Y. C., Wang, C. J., Huang, S. H., Lee, J. W., Chan, Y. C., Chen, H. W., Duh, J. G., and Hsieh, T. E., "The effect of Cr/Zr chemical composition ratios on the mechanical properties of CrN/ZrN multilayered coatings deposited by cathodic arc deposition system." Surf. Coatings Technol., 2013, 231, 247–252.

[14] Wang, M. X., Zhang, J. J., Liu, Q. X., and LI, D. J., "Magnetron sputtering deposition

[DOI: 10.22068/ijmse.2482]

of polycrystalline CrN/ZrN superlattice coatings." Surf. Rev. Lett., 2006, 13, 173–177.

[15] Samim, P. M., Fattah-alhosseini, A., Elmkhah, H., Imantalab, O., and Nouri, M., "A study on comparing surface characterization and electrochemical properties of single-layer CrN coating with nanostructured multilayer ZrN/CrN coating in 3.5 wt.% NaCl solution." Surfaces and Interfaces, 2020, 21, 100721.

[16] Maksakova, O. V., Pogrebnjak, O. D., and Beresnev, V. M., "Features of Investigations of Multilayer Nitride Coatings Based on Cr and Zr." Usp. Fiz. Met., 2018, 19, 25–48.

[17] Vengesa, Y., Fattah-alhosseini, A., Elmkhah, H., Imantalab, O., "Effects of the Post-Deposition Annealing Treatment on the Electrochemical Behavior of TiN Coatings Deposited by CAE-PVD Method." Iranian Journal of Materials Science and Engineering, 2021, 18, 1-12.

[18] Imantalab, O., Fattah-alhosseini, A., "Electrochemical and passive behavior of pure copper fabricated by accumulative roll bonding (ARB) process." J. Materi. Eng. and Perform., 2015, 24, 2579–2585.

[19] Ye, Q. W., Li, Y., Zhang, M. Y., Zhang, S. Z., Bi, Y. J., Gao, X. P., and He, Y. Y., "Electrochemical behavior of (Cr, W, Al, Ti, Si)N multilayer coating on nitrided AISI 316L steel in natural seawater." Ceram. Int., 2020, 46, 22404–22418.

[20] Wang, L., Wang, M., and Chen, H., "Corrosion mechanism investigation of TiAlN/CrN superlattice coating by multi-arc ion plating in 3.5 wt% NaCl solution." Surf. Coatings Technol., 2020, 391, 125660.

[21] Er, D., Taghavi Pourian Azar, G., Kazmanlı, K., and Ürgen, M., "The corrosion protection ability of TiAlN coatings produced with CA-PVD under superimposed pulse bias." Surf. Coatings Technol., 2018, 346, 1–8.

[22] Bayón, R., Igartua, A., Fernández, X., Martínez, R., Rodríguez, R. J., García, J. A., de Frutos, A., Arenas, M. A., and de Damborenea, J., "Corrosion-wear behaviour of PVD Cr/CrN multilayer coatings for gear applications." Tribol. Int., 2009, 42, 591–599.

[23] Ebrahimi, A., Esfahani, H., Fattah-alhosseini, A., and Imantalab, O., "In-vitro electrochemical study of TiB/TiB_2 composite coating on titanium in Ringer's solution." J. Alloys Compd., 2018, 765, 826–834.

[24] Zhu, S., Chen, L., Wu, Y., Hu, Y., Liu, T., Tang, K., and Wei, Q., "Microstructure and corrosion resistance of Cr/Cr_2N multilayer film deposited on the surface of depleted uranium." Corros. Sci., 2014, 82, 420–425.

[25] Mohamadian Samim, P., Fattah-alhosseini, A., Elmkhah, H., and Imantalab, O., "A study on the corrosion resistance of ZrN/CrN multilayer nanostructured coating applied on AISI 304 stainless steel using Arc-PVD method in 3.5 wt% NaCl solution." Mater. Res. Express, 2019, 6, 126426.

[26] Gholami, D., Imantalab, O., Naseri, M., Vafaeian, S., and Fattah-alhosseini, A., "Assessment of microstructural and electrochemical behavior of severely deformed pure copper through equal channel angular pressing." J. Alloys Compd., 2017, 723, 856–865.

[27] Escrivà-Cerdán, C., Blasco-Tamarit, E., García-García, D. M., García-Antón, J., and Guenbour, A., "Effect of potential formation on the electrochemical behaviour of a highly alloyed austenitic stainless steel in contaminated phosphoric acid at different temperatures." Electrochim. Acta, 2012, 80, 248–256.

[28] Hamadou, L., Aïnouche, L., Kadri, A., Yahia, S. A. A., and Benbrahim, N., "Electrochemical impedance spectroscopy study of thermally grown oxides exhibiting constant phase element behaviour." Electrochim. Acta, 2013, 113, 99–108.

[29] Escrivà-Cerdán, C., Blasco-Tamarit, E., García-García, D. M., García-Antón, J., Akid, R., and Walton, J., "Effect of temperature on passive film formation of UNS N08031 Cr-Ni alloy in phosphoric acid contaminated with different aggressive anions." Electrochim. Acta, 2013, 111, 552–561.

[30] Aperador, W., Plaza, M., and Ruiz, E., "Characterization and corrosion behavior of multilayer $[TiN/TiCN]_n$ growth on AISI

[DOI: 10.22068/ijmse.2482]

316LVM steel." Appl. Mech. Mater., 2014, 598, 13–17.
[31] Chipatecua, Y. L., Olaya, J. J., Arias, D. F., Y.L. Chipatecua a, J.J. Olaya, D. F. A., Chipatecua, Y. L., Olaya, J. J., and Arias, D. F., "Corrosion behaviour of CrN/Cr multilayers on stainless steel deposited by unbalanced magnetron sputtering." Vacuum, 2012, 86, 1393–1401.
[32] Rashmi, S., Elias, L., and Chitharanjan Hegde, A., "Multilayered Zn-Ni alloy coatings for better corrosion protection of mild steel." Eng. Sci. Technol. an Int. J., 2017, 20, 1227–1232.
[33] Zhou, Y., Asaki, R., Soe, W.-H. H., Yamamoto, R., Chen, R., and Iwabuchi, A., "Hardness anomaly, plastic deformation work and fretting wear properties of polycrystalline TiN/CrN multilayers." Wear, 1999, 236, 159–164.
[34] Rengifo, E. H., Caicedo, J., and Ortiz, C., "Mechanical and Tribological Properties Evolution of $[Si_3N_4/Al_2O_3]_n$ Multilayer Coatings." Tribology in Industry, 2021, 43, 23-39.
[35] Postolnyi, B. O., Beresnev, V. M., Abadias, G., Bondar, O. V., Rebouta, L., Araujo, J. P., and Pogrebnjak, A. D., "Multilayer design of CrN/MoN protective coatings for enhanced hardness and toughness." J. Alloys Compd., 2017, 725, 1188–1198.
[36] Kumar, D. D., Kumar, N., Kalaiselvam, S., Dash, S., and Jayavel, R., "Wear resistant super-hard multilayer transition metal-nitride coatings." Surfaces and Interfaces, 2017, 7, 74–82.
[37] Tsai, Y. and Duh, J., "Tribological behavior of CrN / WN multilayer coatings grown by ion-beam assisted deposition." Surf. Coatings Technol., 2006, 201, 4266–4272.
[38] Xu, X., Su, F., and Li, Z., "Tribological properties of nanostructured TiAlN/W_2N multilayer coating produced by PVD." Wear, 2019, 430, 67–75.
[39] Zhang, Q., Xu, Y., Zhang, T., Wu, Z., and Wang, Q., "Tribological properties, oxidation resistance and turning performance of AlTiN/AlCrSiN multilayer coatings by arc ion plating." Surf. Coatings Technol., 2018, 356, 1–10.
[40] Mileti, A., Panjan, P., Cekada, M., Kova, L., and Dra, G., "Nanolayer CrAlN / TiSiN coating designed for tribological applications." Ceram. Int., 2021, 47, 2022-2033.
[41] Kong, Y., Tian, X., Gong, C., and Chu, P. K., "Enhancement of toughness and wear resistance by CrN / CrCN multilayered coatings for wood processing." Surf. Coat. Technol., 2018, 344, 204–213.
[42] Holmberg, K., Coatings Tribology Properties, Mechanisms, Techniques and Applications in Surface Engineering, 2nd Edition, Elsevier, 2009.
[43] Gilewicz, A. and Warcholinski, B., "Tribology International Tribological properties of CrCN/CrN multilayer coatings." Tribiology Int., 2014, 80, 34–40.

[DOI: 10.22068/ijmse.2482]